Observing and Understanding the Ultrafast Photochemistry in Small Molecules: Applications to Sunscreens

Lewis A. Baker* and Vasilios G. Stavros†

Department of Chemistry, University of Warwick, Coventry, CV4 7AL, UK.

Lewis A. Baker studied Physics at the University of Warwick, obtaining an MPhys in 2013. He went on to study Mathematical Biology and Biophysical Chemistry at the University of Warwick *Molecular Organisation and Assembly in Cells Doctoral Training Centre*, obtaining an MSc in 2014 and proceeding to a PhD. His thesis focusses on understanding biological photoprotection through transient absorption spectroscopy and quantum dynamic simulations.

Vasilios G. Stavros is a Reader at the University of Warwick. He completed his PhD in 1999 at King's College London, working in the group of Professor Helen Fielding and remained at King's for a further three years as an EPSRC postdoctoral research fellow. In 2002, he undertook a postdoctoral position at the University of California Berkeley, working for Professor Stephen Leone. He returned to the UK in 2005 as a Royal Society University Research Fellow. His research is centred on understanding photoprotection and photoactivation mechanisms in biologically related molecules using both gas- and solution-phase pump-probe spectroscopies.

*Electronic address: L.Baker@warwick.ac.uk
†Electronic address: V.Stavros@warwick.ac.uk

Abstract

In this review we discuss the importance of biological and artificial photoprotection against overexposure to harmful ultraviolet radiation. Transient electronic and transient vibrational absorption spectroscopies are highlighted as important tools in understanding the energy transfer in small molecules, with a focus on the application to commercial sunscreens with representative examples given. Oxybenzone, a common ingredient in commercial sunscreens and sinapoyl malate, a biological sunscreen in plant leaves are presented as case studies.

Keywords: Ultraviolet radiation, ultrafast spectroscopy, transient absorption, photoprotection, sunscreens, photochemistry, femtochemistry, oxybenzone, sinapoyl malate.

1 Introduction

Ultraviolet radiation (UVR, ∼400–100 nm) is the most energetic component of the solar spectrum which reaches the Earth, typically subdivided into the UV-A region (400–315 nm), UV-B (315–280 nm), and the most energetic region, UV-C (280–100 nm). These high energy components can cause major disruptions in the biochemistry of life, often in the form of chemical bond breaking. Throughout the development of Earth's atmosphere, the radiation which bombards the Earth's surface has changed dramatically. Around 3 billion years ago when the earliest lifeforms on Earth are known to have existed, the atmosphere likely consisted predominately of carbon dioxide and methane, meaning the solar spectrum reaching the Earth's surface consisted of much UV-C radiation[1]. As such, these early organisms were forced to migrate away from the surface, or develop other mechanisms in order to reduce exposure in order to survive[2]. The latter is particularly important for the earliest complex lifeforms, the first phototrophs, which needed to absorb sunlight for photosynthesis, but be protected against too much UV-C exposure.

Today, the ozone rich stratospheric layer of the Earth's atmosphere absorbs all the UV-C wavelengths, and much of the UV-B, and as a result the solar spectrum reaching Earth's surface comprises of as little as 8% UVR. Though this is a small proportion of the total solar spectrum (especially compared to the early Earth atmosphere), these high energy components still have an extensive impact on the Earth's biosphere. Most notably, >90% of the vitamin-D requirements of the human body are met through UV-B photocatalytic reactions[3]. On the other hand, the negative attributes of UV-B exposure are extensive; deoxyribonucleic acid (DNA) nucleotides and protein manifolds for example can absorb UV-B radiation which can lead to mutations in cells or the disruption of vital biochemical pathways like photosynthesis[4]. Thus exposure to UVR remains in an equilibrium of the so-called *burden of disease*; too little UV-B exposure and important biochemical processes are not active, too much and the prevalence of adverse effects increase.

The remainder of this review is organised as follows: in the ensuing discussion, we focus on the biological photoprotection displayed in humans and some higher order plants. In Section 1.2 we introduce a commonly employed method of sunscreens to provide additional photoprotection and discuss their operation and the current controversies surrounding their use. In Section 1.3 we review the common photophysical processes involved in the

relaxation of photoexcited molecules. In Section 2 we present transient electronic absorption spectroscopy and its vibrational analogue as suitable techniques for observing ultrafast processes. Common data analysis techniques for extracting quantitative information from recorded measurements are reviewed. In Section 3 two case studies are presented from recent work which have utilised transient absorption spectroscopy to understand the ultrafast photophysical processes occurring in a commercial sunscreen molecule as well as a natural biological sunscreen molecule.

1.1 Biological photoprotection

1.1.1 UVR exposure to humans

Negative attributes of UVR exposure. The negative attributes of UVR exposure to humans is extensive and still remains an active area of research. A well known consequence of UV-B overexposure is skin cancer, both non-melanoma *e.g.* basal and squamous cell carcinomas, and malignant melanomas, of which there are estimated 2-3 million and 130,000 cases respectively world-wide, both attributing to the ∼65,000 fatalities from skin cancers alone[5–7]. Less well known examples of skin damage include degenerative changes in cells of the skin, fibrous tissues and blood vessels, all of which have been associated with premature skin-ageing and photodermatoses. Another prevalent example of UVR damage is the eyes where acute effects range from conjunctivitis and retinopathy, to chronic effects including ocular melanoma and cataracts, the latter is responsible for around ∼3 million cases per year globally[7]. The immune system can also become disrupted by UVR overexposure where cell-mediated immunity can become suppressed leading to an increased susceptibility to infections. Furthermore overexposure has been associated with the activation of latent viral infections, *herpes labialis* (cold sores) for example. On the other hand chronic UVR underexposure has been associated with the development of some psychiatric disorders such as seasonal affective disorder and schizophrenia.

Positive attributes of UVR exposure. UV-B radiation behaves as a photocatalyst for the conversion of 7-dehydrocholesterol to previtamin D_3, an early step in the synthesis of vitamin D[8]. In fact, UV-B mediated production of vitamin D constitutes to more than 90% of the total vitamin D requirements of the body[3]. Thus UV-B underexposure can lead to a deficiency in vitamin D which has a range of far-reaching consequences on the body. Early development of bones for example require vitamin D which otherwise can lead to disease such as rickets and skeletal disease[3;8]. Other beneficial effects of adequate UVR exposure such as a lower incidence of some cancers, *e.g.* Non-Hodgkins lymphoma have also been suggested[5].

Maintaining an equilibrium. The human body has a number of mechanisms at its disposal in order to prevent, protect, or repair damage from the adverse effects of UVR over- or underexposure. For example, UVR induced DNA damage can be repaired by nucleotide/base excision or, in the case of severely damaged cells, apoptosis can prevent the replication of a damaged genome[9]. These mechanisms are reserved as a 'last resort' to DNA damage; skin pigmentation is the primary photoprotective mechanism found in humans. Skin pigmentation works by absorbing harmful UVR before it has had chance to interact with DNA or other UV sensitive constituents of a cell. This pigmentation is made up of melanins, a class of UV absorbing molecules which polymerise into chains and are deposited inside a cell above

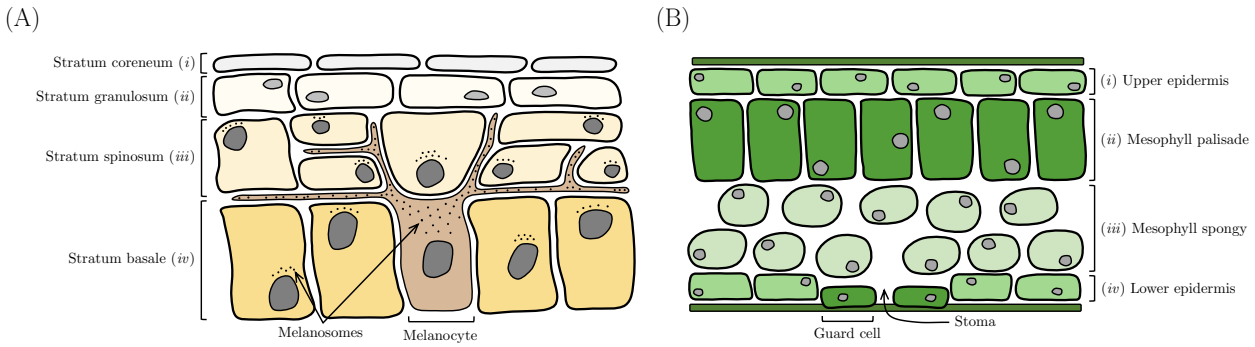

Figure 1: (A) Schematic of the layers found in the skin epidermis. (*i*) The first layer of the epidermis is the stratum coreneum, which consists of a protective layer of dead keratinocytes. (*ii*) The stratum granulosum is a layer of keratinocytes migrating towards the stratum coreneum, which in the process lose their nucleus and organelles. (*iii*) The stratum spinosum is the thickest layer of the epidermis, packed with keratinocytes. (*iv*) The bottom layer of the epidermis is the stratum basale layer. This layer consists of keratinocytes and melanocytes. The melanocytes produce melanosoma, which are packed with the UV absorbing pigment melanin. These melanosoma are distributed throughout the keratinocytes within the basale and spinosum layers and preside predominately around the cell's nucleus, in the path of incoming UVR. (B) Schematic of the layers found in a typical plant leaf. (*i*) The upper epidermis consists of cells with UV-absorbing metabolites, synthesised *via* the phenylpropanoid pathway, providing photoprotection to lower lying layers. (*ii*) The mesophyll palisade layer contains a high proportion of chlorophyll, responsible for the majority of light harvesting from the sun for photosynthesis. (*iii*) The mesophyll spongy is a dispersed layer of cells allowing room for the exchange of gases required for photosynthesis. (*iv*) The lower epidermis contains cell-regulated openings (stoma) in the leaves by guard cells, allowing for photosynthetic gases to be imported (CO_2) or exported (O_2).

its nucleus, in the path of incoming UVR. The primary melanins are eumelanin, a black-brown pigment and pheomelanin, a yellow-reddish pigment, both of which are synthesised inside specialised cells called *melanocytes*[10]. Melanocytes are distributed throughout the skin, predominately in the stratum basale layer, see Figure 1(A). They synthesise membrane bound organelles full of polymerised melanin called *melanosoma*, which are transported into surrounding cells (keratinocytes) throughout the basale and spinosum layers. The skin pigmentation therefore will depend on the number, size, distribution, morphology and melanin content of the melanosoma and melanocytes[11]. These properties are regulated by a set of genes which can be up-regulated or down-regulated in response to a change in UVR exposure in a process called *melanogenesis*[9;10]. Thus, in environments where UVR exposure is greater than the skin is protected against, melanogenesis is up-regulated to increase the distribution of eumelanin in the skin keratinocytes (predominately in the basale layer), which is commonly referred to as 'tanning'. Conversely, if UVR exposure is too low, melanogenesis is down-regulated to decrease eumelanin distribution so that sufficient vitamin D can be synthesised. Melanogenesis is therefore an important process for maintaining an optimal balance in the burden of disease, illustrated in Figure 2. An issue remains; although there is a regulated pathway to respond to changes in incident UVR, it is a delayed response ($\sim$3-5 days after UVR overexposure), after which photodamage could have already occurred, with any intermediate tanning affording almost no additional protection at all[12;13]. Principally the same as with humans, plants exhibit a burden of disease curve in response to UVR with a regulated pathway which attempts to maintain an optimal equilibrium, see Figure 2.

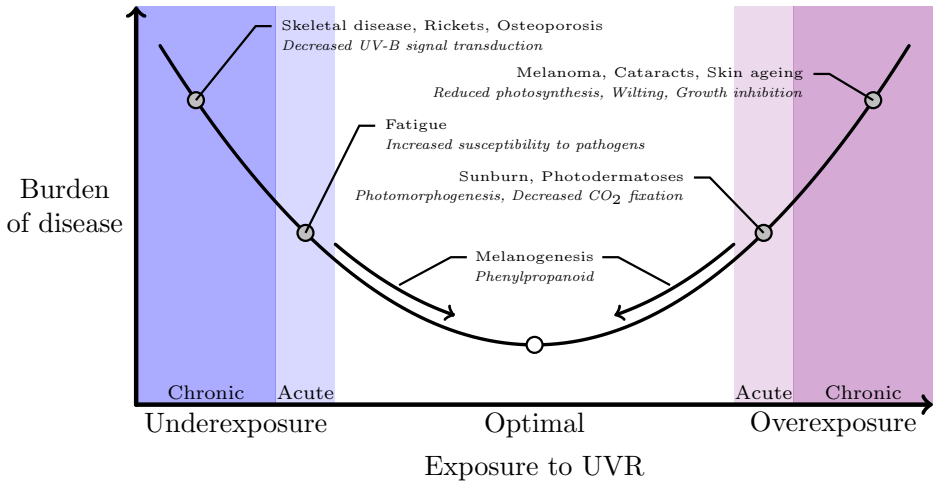

Figure 2: A representation of the probability of disease incidence, with common ailments associated with UVR overexposure (violet) or underexposure (blue) in humans (*and in italics for plants*). For both humans and plants there are regulated pathways which attempt to maintain a balance between the burden of disease associated with either extreme of UVR exposure, keeping it close to the optimal position and thus the lowest incidence of disease.

1.1.2 UV exposure to plants

Negative attributes of UVR exposure. Plant life has achieved phenomenal resilience to a variety of living conditions and an ability to adapt to dynamic changes in its habitat, of which UVR exposure is just one example. Like humans however, overexposure to UVR, and in particular UV-B radiation can have detrimental effects on a plant's ability to survive. Perhaps the most profound effect is through damage to DNA either by direct photodamage, or indirectly *via* the generation of reactive oxygen species which subsequently interact with DNA nucleotides[14;15]. This can lead to genetic mutations which, unless repaired (the probability of which decreases with increased UVR exposure) will cause cells to either replicate a damaged genome or to undergo apoptosis and die. UVR is also known to damage photosynthetic machinery, specifically enzymatic control of photosystem II which can dramatically reduce photosynthetic efficiency, similarly a reduction in pollen fertility is known to occur in some plants[15]. Another noticeable change brought on by UVR overexposure is photomorphogenesis, whereby a plant's leaves change morphology due to UVR *e.g.* the epidermis may become thicker, and has consequences which include an increased susceptibility to invading pathogens[14;15].

Positive attributes of UVR exposure. UV radiation, in particular UV-B radiation behaves as a signal transducer for an enormous array of processes; some, as described above, are degenerative to a plant's survival but many initiate or regulate gene responses which are vital for survival[14]. UV-B radiation stimulates the expression of genes responsible for DNA repair, a noteworthy example is the use of UV-A and enzymatic control for the repair of photodamaged DNA nucleotides. Contrary to the negative attributes of photomorphogenesis described above, some changes to leaf morphology can deter pests, significantly increasing survival rates.[14;15]

Maintaining an equilibrium. Like with humans, plants are continuously trying to main-

tain a balance in the burden of disease *cf.* Figure 2. They require sunlight to carry out photosynthesis and thus have to be subjected to some UVR in the daily solar spectrum, but clearly too much UVR can be damaging. Similar to melanogenesis in humans, plants have a regulated biochemical pathway which can be up-regulated and down-regulated in response to UVR exposure, called the *phenylpropanoid pathway*[16]. This pathway is responsible for the synthesis of a rich source of metabolites used in a myriad of biochemical processes throughout a plant. With respect to photoprotection, the most prominent metabolites are sinapate esters such as sinapoyl malate which are deposited in the vacuoles of cells in the upper epidermis of leaves. These behave as UV-B filters, absorbing and subsequently dissipating UV energy before it reaches sensitive cells in the mesophyll palisade layers, see Figure 1(B). Thus, mirroring melanogenesis in humans cells, in environments of high UVR, the phenylpropanoid is up-regulated to synthesise more sinapate esters to deposit in the upper epidermis[16].

1.2 Artificial photoprotection: sunscreens

Both humans and plants display a multitude of effects to UVR exposure, where a careful balance is struck between over- and underexposure through regulated pathways, continuously responding to environmental changes in UVR levels. Focussing on human photoprotection, where a delayed tanning response can mean UVR damage has already occurred, pre-emptively protecting the skin to UVR overexposure is likely to reduce overall photodamage. This has become increasingly important given today's availability of tourism[17], and attitudes towards tanning[13], meaning tourists for example, are increasingly subjected to UVR levels well beyond their skin's current photoprotection. There are many ways to protect oneself from UVR overexposure, clothing, sunglasses, seeking shade and educating people are all examples of effective ways to reduce exposure but these are not always possible for a variety of reasons *e.g.* the want to sunbathe on holiday, which has led to the widespread use of sunscreens as the almost universal primary artificial photoprotection (*i.e.* in addition to any biological photoprotection discussed in Section 1.1).

Sunscreens are applied to the upper epidermis of the skin and work in combination with biological photoprotection by absorbing or scattering UVR and stopping it from reaching the UV-sensitive areas of the skin. Typically sunscreens consist of a combination of *organic filters* which absorb radiation and subsequently dissipate it through nondestructive pathways, internally or to surrounding molecules[18]. The most common examples are aromatic molecules which often provide $\pi^* \leftarrow \pi$ transitions that are accessible by UVR, see Figure 3(A). In combination to organic filters, *inorganic scatterers* provide large spectral coverage across UVR wavelengths by scattering (as well as absorbing) incoming UVR away from skin cells. Common examples of inorganic scatterers are nanoparticles of titanium dioxide and zinc oxide[19], see Figure 3(B). Thus a combination of organic filters and inorganic scatterers can provide broad spectral coverage across UV wavelengths; this is the primary rationale for commercial sunscreens. However, other considerations are taken into account in sunscreen development. For example, the texture, colour and smell of a sunscreen product is important as the user is unlikely to use or reapply sunscreens if they are not cosmetically pleasing. Ultimately this means that sunscreens consist of many 10's of different compounds to provide an efficient photoprotective, cosmetically pleasing and financially viable product. Another consideration needs to be taken when selecting a molecule for a sunscreen; given the great

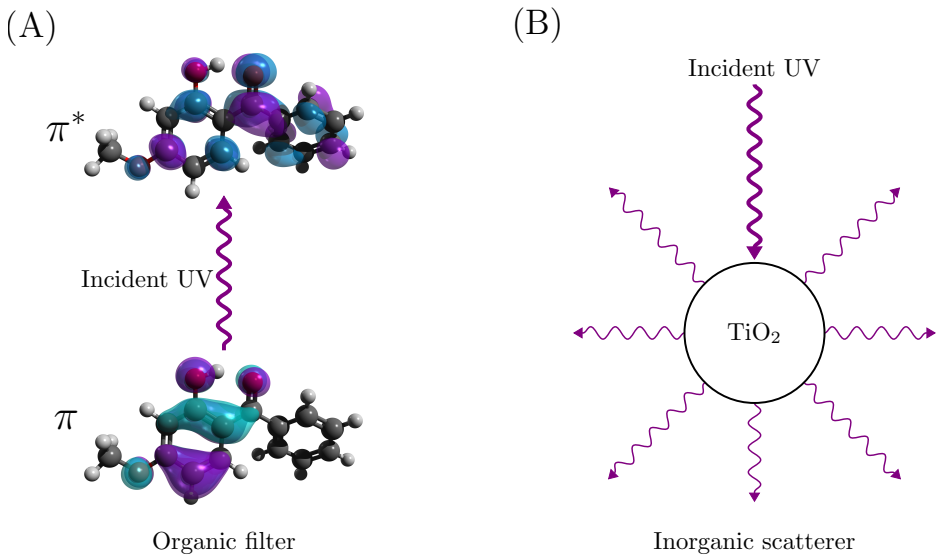

Figure 3: (A) Oxybenzone, a common organic filter used in commercial sunscreens exhibits a strong $\pi^* \leftarrow \pi$ transition when excited by UV radiation, responsible for its broadband absorption profile across the UV region[20–22]. In general, organic filters absorb UVR and dissipate it before it can reach sensitive skin cells. (B) An extensively used inorganic scatterer in commercial sunscreens, titanium dioxide (TiO_2). Unlike organic filters, inorganic scatterers also provide photoprotection through scattering UVR away from the skin, as well as absorbing.

photon flux arriving at one's skin on a typical day, any good filtering sunscreen molecule needs to not only absorb harmful UVR, but also needs to dissipate the energy on ultrafast timescales (picoseconds, 1 ps = 10^{-12} seconds, to femtoseconds, 1 fs = 10^{-15} seconds) efficiently such that it is ready to absorb another UV photon, otherwise the sunscreen would not provide photoprotection for any tangible time, or, many layers of sunscreen would be required for any photoprotection.

A problem however exists in that these selection criteria do not necessarily lead to a skin-friendly product. For example, if a sunscreen molecule dissipated the absorbed UV energy through destructive pathways, *e.g.* radical formation (or other photophysical processes, described in Section 1.3), it can lead to subsequent damaging interactions with surrounding cells. This, coupled with a limited literature with conflicting studies, has led to what is commonly referred to as the "sunscreen controversy"[23]. Essentially it revolves around the question *do sunscreens contribute to the adverse effects of UV exposure they are supposed to protect against?* A clear example of this involves a molecule which has found use in commercial sunscreen products, the organic filter oxybenzone ((2-Hydroxy-4-methoxyphenyl)-phenylmethanone; see Figure 3). Oxybenzone has been shown to be an effective sunscreen with respect to its ability in absorbing UVR across the UV-A and UV-B regions dissipating it on ultrafast timescales[24;25]. Contrary to this, oxybenzone has been suggested to form a potentially adverse photoproduct after being excited by UVR[26]. Furthermore, there is evidence to suggest that oxybenzone may behave as an endocrine disrupter and a photoallergen[23;27]. Thus, this is a present example of how even commonly used sunscreens are at a point of contention with regards to the *net* positive protection they provide.

From a photophysical perspective, we are interested in answering two questions. The

first is, *by what mechanism does a sunscreen molecule dissipate its energy after an initial UV photoexcitation?*. The second is, *how quickly does it complete this mechanism?* Answering these questions allow for the efficiency of a sunscreen molecule to be described quantitatively and begins to resolve some of the issues raised in the sunscreen controversy.

1.3 Photochemistry

Photochemistry is the field of study describing the chemical processes occurring in molecular systems after excitation by electromagnetic radiation. Given that any excess energy a molecule possesses typically makes it less stable, it will always act to lower its total energy to a minimum, referred to as its ground electronic state, S_0. Here 'S' denotes a singlet state whilst 'T' denotes a triplet state, the difference being the electron spin multiplicity of the state being 1 and 3 respectively. Depending on the energy of the incident photon, and the transitions available in a molecular system, an initial photoexcitation can force the molecule into higher energy electronic states, referred to as S_n; $n \geq 1$. The first question posed in the previous section can now be refined as: how does the excited state molecule dissipate energy such that the molecular system goes from $S_n \rightarrow S_0$, and, if the molecule does not return to S_0, what *does* it do? Photophysically, there are numerous possibilities by which a molecular system may dissipate its energy, depending on for example, the distribution of charges within the molecule, the strength of vibrational couplings between electronic states and the influence of the environment (*e.g.* solvent). A summary of the typical photophysical processes which may occur after photoexcitation is given in Figure 4.

Nonradiative processes. There is a continuum of vibrational states, ν_m, associated with each electronic state with these larger molecular systems, with ν_0 the ground vibrational

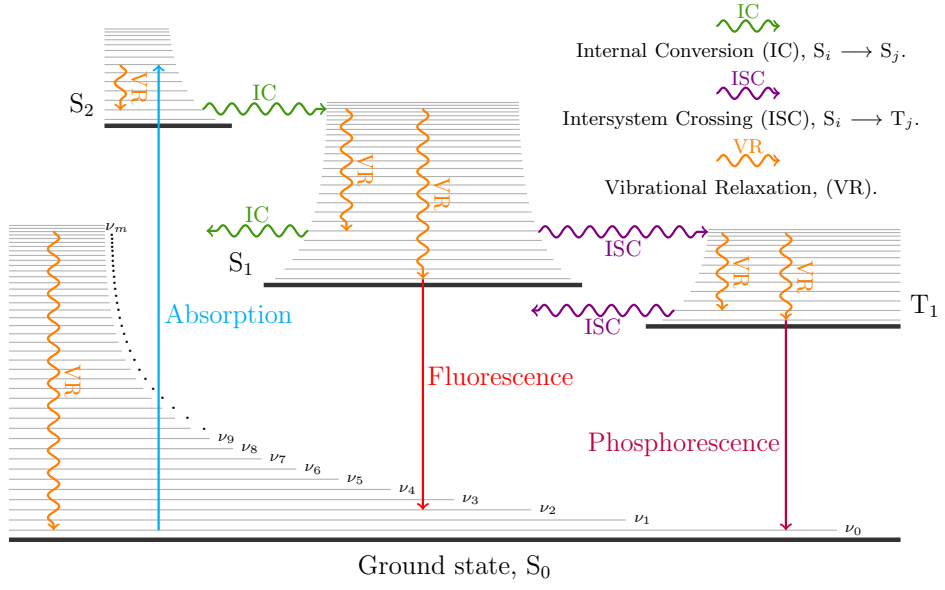

Figure 4: A summary of the important photophysical processes which occur after a molecule is photoexcited from its electronic ground state, S_0, and vibrational ground state, ν_0, to an excited vibronic state, *i.e.* excited electronic (S_n; $n \geq 1$) and vibrational state (ν_m; $m \geq 1$). Following this, there are a number of radiative ($\rightarrow$) and nonradiative ($\rightsquigarrow$) processes a molecule may undergo to dissipate its excess energy.

state and ν_m; $m \geq 1$ the excited vibrational states. This means an initial absorption event can result in a molecule residing in an excited vibrational state (ν_m) as well as an excited electronic state (S_n), often referred to as a vibronic transition. The molecule may relax to a lower vibrational state by *vibrational relaxation*, through collisions with other molecules, or *via* vibrational energy redistribution within the molecule itself. Vibrational states between two electronic states with the same spin multiplicity (*i.e.* $S_i \rightarrow S_j$ or $T_i \rightarrow T_j$) may couple to provide a route for energy transfer within a molecule, this is called *internal conversion* (IC). Conversely, for vibrational states coupling electronic states of different spin multiplicity (*i.e.* $S_i \rightarrow T_j$ or $T_i \rightarrow S_j$), energy transfer is referred to as *intersystem crossing* (ISC). Bond dissociation is another process which might occur, one which would want to be avoided in sunscreen molecules as this leads to the formation of photoproducts which are likely to initiate damage to surrounding cells or to reduce the overall efficiency of the applied sunscreen product.

Radiative processes. An excited state molecule may relax to a lower electronic state if there is good (Franck-Condon) overlap between the wavefunctions of the vibrational state of the upper and lower electronic states. This results in the release of a photon with energy matching the difference in initial and final states, which is the commonly observed process of *fluorescence*. This is true when the initial and final states have the same spin multiplicity; if the radiative transition is between states of different spin multiplicity the process is known as *phosphorescence*. Additionally, phosphorescence can be quenched due to the excited state lifetime, discussed below.

Timescales. Aside from the availability of specific transitions, the timescales of these typical processes are key in determining the mechanisms molecules relax by since they will compete with different pathways, for example, if both IC and ISC pathways are accessible, the majority of an ensemble of molecules will relax preferentially *via* IC than ISC since ISC is a spin-forbidden (and therefore less probable) transition. The typical timescales of the processes discussed and summarised in Figure 4 are given in Table 1[28]. Thus the dominant processes which a molecule relaxes by will be directly responsible for its efficiency as a sunscreen for two reasons. The first is that the quickest pathways will reduce the time for the photoexcited molecule to become available to absorb UVR again. The second is that some pathways will be detrimental to the safety of a molecule to be used as a sunscreen. For example, if fluorescence

Table 1: The typical time scales for the common photophysical processes which occur after photoexcitation [28].

Process	Time taken / s
Absorption	10^{-18} – 10^{-15}
Bond dissociation	10^{-15} – 10^{-12}
Vibrational relaxation	10^{-12} – 10^{-10}
Internal conversion	10^{-11} – 10^{-9}
Intersystem crossing	10^{-10} – 10^{-8}
Fluorescence	10^{-10} – 10^{-7}
Phosphorescence	10^{-6} – 1

is a dominant pathway, then radiation (albeit at a lower energy) will be expelled into the surrounding environment which can be damaging to the skin cells, or, if bond dissociation is a favoured pathway, this could lead to damage through subsequent chemical reactions (*e.g.* radicals).

The timescales involved in the processes which are likely to be in operation in efficient sunscreen molecules are therefore ultrafast, occurring on femtosecond and picosecond timescales. In the next section we introduce the experimental technique, transient absorption spectroscopy, as a key tool to probe the processes and timescales of the relaxation mechanisms in sunscreen molecules as an important step in beginning to answer questions about the applicability, safety and efficiency of these molecules.

2 Transient absorption spectroscopy

2.1 Experimental methodology

The historic measurements by Ahmed Zewail's group in 1985[29] (and later refined in 1987[30]) of the bond breaking reaction, $ICN^* \rightarrow I + CN$, is widely attributed to the birth of femtochemistry[31], where for the first time, reaction dynamics (*i.e.* the formation of the I and CN fragments) could be observed on a femtosecond timescale. Since then, this pioneering technique used to study simple dissociation reactions has been applied to a plethora of physical, chemical and biological systems, with examples ranging from understanding fundamental quantum dynamics[32] to energy transfer in photosynthetic antennas[33] and porphyrin biomimics[34]. The key in all these experiments is the use of ultrashort lasers pulses, which typically have a duration of <100 fs, in what is known as a *pump-probe* setup. In the ensuing section we introduce how a pump-probe experiment which uses ultrafast laser pulses can be used to understand how sunscreen molecules relax after UV photoexcitation, and resolve the timescales of the processes involved. Importantly, we focus on sunscreen molecules in the solution phase which more closely mimics the environment of commercial sunscreen products.

One laser pulse is used to photoexcite a molecule at a particular wavelength, called the *pump* pulse, in the case of sunscreens molecules, this wavelength will be in the UV region to simulate the conditions sunscreens are used in. Another laser pulse, drawn from a white light continuum consisting of wavelengths across the UV and visible regions (∼300–800 nm), is used to measure the UV-visible excited state absorption profile of the photoexcited molecule, called the *probe* pulse. The result is essentially a UV visible absorption spectrum of the excited state molecule. By altering the time at which the probe pulse arrives at the molecule relative to the pump pulse, 'snapshots' of the *static* excited state absorption profile can be recorded and used to produce a *dynamic* absorption profile (analogous to the many single pictures used to make a video). The difference in arrival times of the pump and probe is termed the *time delay*, Δt, where $\Delta t = 0$ describes perfect temporal arrival synchronisation, also referred to as 'time-zero', and $\Delta t > 0$ describes the probe pulse arriving *after* the pump pulse. Typically time delays up to many nanoseconds (1 ns = 10^{-9} seconds) in increments as small as 10 fs are used to capture snapshots of the excited state absorption profile across the entire ultrafast timescale.

Ultrashort pulse generation. As briefly described, to resolve ultrafast processes, ultrashort

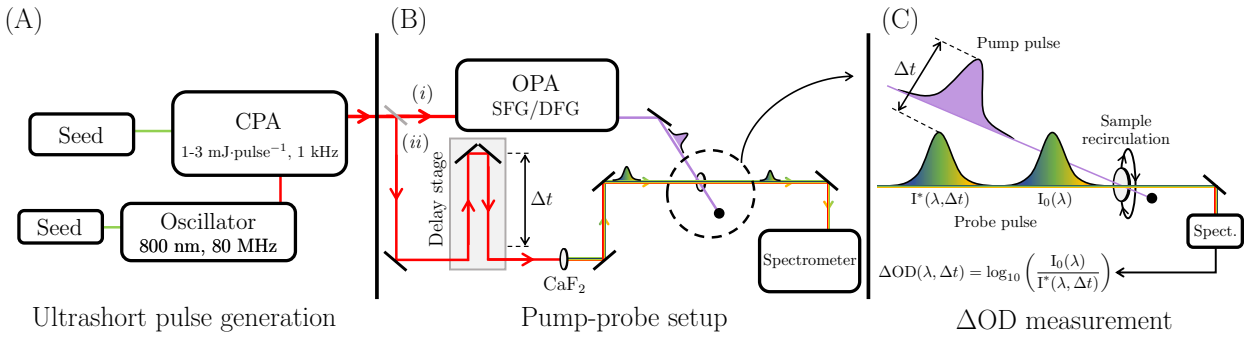

Figure 5: Schematic representation of a typical transient absorption spectroscopy experimental setup. (A) A mode-locked Ti:sapphire laser outputs 800 nm pulses with a repetition rate of ∼80 MHz. These are energetically weak (∼1-3 nJ per pulse) so they are used to seed a Ti:sapphire chirp regenerative amplifier (CPA). The CPA amplifies and compresses one in 80000 seed pulses and outputs 800 nm, ∼1-3 mJ per pulse at a repetition rate of 1 kHz, with a pulse duration of ∼45 fs. (B) The 800 nm output is split into two beams. (*i*) The majority of the output from the CPA seeds either optical parametric amplification (OPA), sum frequency generation (SFG) or difference frequency generation (DFG) which is used for the pump pulses. (*ii*) A small portion of the output of the CPA is focussed inside a CaF_2 crystal for white light generation to be used as the probe pulse for transient electronic absorption spectroscopy. For transient vibrational spectroscopy, broadband infrared pulses can be generated *via* a suitable nonlinear medium which are used as the probe pulses. A delay stage is used to change the path length of the probe relative to the pump to introduce a specific time delay, Δt, between them. Both pump and probe are overlapped inside a flow-through cell where the sample is recirculated. A polariser is often used in the probe path to rotate the polarisation of the probe relative to the pump for magic angle (∼54.7°) spectroscopy. (C) The transmission of the probe pulse is recorded for both a pumped ($I^*(\lambda, \Delta t)$) and unpumped sample ($I_0(\lambda)$), for a range of pump-probe time delays. From these measurements the change in optical density, ΔOD, is calculated for each wavelength at every time delay, the result is the commonly reported transient absorption spectrum.

laser pulses are required. A common method for ultrashort pulse generation is through the use of Ti:sapphire lasers which exhibit strong lasing transitions around 800 nm, illustrated in Figure 5(A)[33;35]. Typically, a green seed laser optically pumps a Ti:sapphire oscillator. This oscillator is mode-locked around 800 nm and releases pulses at a repetition rate of ∼80 MHz *via* an optical switch[36]. Typically, one in 80000 of these pulses is selected as a 800 nm seed for amplification (*i.e.* a repetition rate of 1 kHz). Inside the amplifier (*e.g.* a Ti:sapphire chirp regenerative amplifier, optically pumped by another green seed laser) this 800 nm seed pulse is amplified by factor of $\sim 10^6$ and compressed to about ∼45 fs in duration[36].

Pump-probe setup. The ultrashort 800 nm pulses are used to generate both the pump and probe pulses as illustrated in Figure 5(B) by splitting them into two beams (*i*) and (*ii*) for the pump and probe pulse generation respectively. (*i*) To generate the pump pulses, the 800 nm pulses seed an optical parametric amplifier which can generate tunable laser pulses of a variety of wavelengths (in particular for sunscreens, across the UV regions). Another option is to use sum frequency generation or difference frequency generation to produce specific wavelengths (*e.g.* the second harmonic, 400 nm, or the third harmonic, 267 nm)[37]. The result of either of these options is a consistent source of pump pulses at the wavelength required for photoexcitation. (*ii*) The probe pulses on the other hand are generated by focussing 800 nm pulses into a suitable nonlinear medium, *e.g.* CaF_2, which produces pulses with a broad bandwidth referred to as white light generation (WLG), typically consisting of wavelengths between ∼300–800 nm which are subsequently used as the probe pules. Because

of the use of UV-visible wavelengths this technique is often referred to as *transient electronic absorption spectroscopy*. Importantly, broadband infrared pulses may be used in place of white light pulses which probe the vibrational modes of the molecule[38], called *transient vibrational absorption spectroscopy*. Within this line, before WLG, the 800 nm pulses travel along a delay stage which consists of a motorised retro-reflector that introduces a specified Δt into the probe path. Furthermore, a polariser can be placed in this path for magic angle (54.7°) pump-probe spectroscopy. Both pump and probe pulses are focussed into the sample with any pump pulses not absorbed by the sample collected in a beam dump, whereas residual probe pulses are collimated and coupled into a spectrometer. One caveat is required in the discussed experimental set up. The delay stage can in principle be introduced in either the pump or probe beam path, with the latter being used here.

ΔOD *measurement*. The actual reported measurements from these experiments are the changes in optical density ΔOD, which for all probe wavelengths and all Δt, results in a transient absorption spectrum (TAS), see Figure 5(C). The calculation of ΔOD is as follows. The spectral absorption of the probe by a molecule *without any photoexcitation* results in a transmitted intensity for each probe wavelength, λ, of $\mathrm{I}_0(\lambda)$. The molecule is then photoexcited with a pump pulse. After a time Δt another probe pulse is absorbed by the *photoexcited molecule*, which results in a transmitted intensity for each probe wavelength, for the given Δt, of $\mathrm{I}^*(\lambda, \Delta t)$. The logarithmic quotient of these measurements is a dimensionless, instrument independent quantity known as the change in optical density, ΔOD:

$$\Delta\mathrm{OD}(\lambda, \Delta t) = \log_{10}\left(\frac{\mathrm{I}_0(\lambda)}{\mathrm{I}^*(\lambda, \Delta t)}\right). \tag{1}$$

Another noteworthy experimental detail is that the sample which is to be studied is recirculated from a reservoir. This ensures that subsequent measurements will use a fresh sample, particularly important if the sample being studied degrades after photoexcitation. The recorded TAS is the total signal from the photoexcited molecule, *i.e.* a convolution of all possible sources of a change in optical density. There are four main processes which manifest themselves as a change in optical density in a typical experiment[33], illustrated in Figure 6.

Ground state bleach. The pump pulse photoexcites a fraction of the molecules in a sample to an excited state, thus the number of molecules in the ground state decreases. This leads to a decrease in the ground state absorption compared the absorption of a unpumped sample. Therefore, the transmission intensity of the probe in the pumped sample is greater than the unpumped sample, *i.e.* $\mathrm{I}^*(\lambda, \Delta t) > \mathrm{I}_0(\lambda)$ so the quotient in Eq. 1 is < 0. Thus a ground state bleach signal manifests as a *negative* ΔOD signal.

Stimulated emission. One probe photon may initiate the stimulated emission of an additional photon from an excited state. In the pumped sample, there are more molecules in an excited state which may undergo stimulated emission compared to the unpumped sample. Thus the intensity detected from stimulated emission is greater in the pumped sample than the unpumped sample hence stimulated emission manifests as a *negative* ΔOD signal.

Excited state absorption. In the pumped sample, the molecules will absorb wavelengths of the probe pulse corresponding to optically allowed transitions to higher electronic states (S_n), thus will decrease the transmission intensity of the probe pulse. In the unpumped sample, these same transitions will not be accessible thus the transmission intensity of the

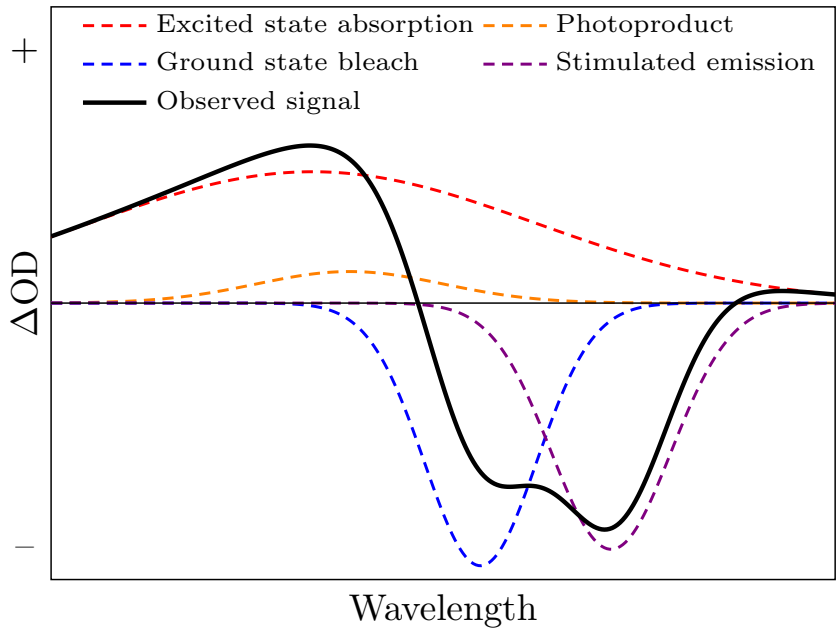

Figure 6: Schematic of the typical components which contribute to the measured transient absorption spectrum, for a particular Δt.

unpumped sample will be greater than in the pumped sample, *i.e.* $I^*(\lambda, \Delta t) < I_0(\lambda)$ so the quotient in Eq. 1 is > 0. Thus an excited state absorption signal manifests as a *positive* ΔOD signal.

Photoproduct absorption. After photoexcitation, a molecule may relax through a mechanism which does not result in its original state forming a photoproduct, for example, long-lived triplet states, fragmentation into two or more fragments or isomerisation to a stable state. In this case, photoproducts may absorb probe wavelengths, reducing the transmission intensity compared to the unpumped sample where there are no photoproducts. Hence photoproduct absorption manifest as a *positive* ΔOD signal.

2.2 Analysis of the transient absorption spectrum

Knowing what each contribution to the ΔOD has on the resulting TAS helps to assign spectral features to specific processes. For example, the very existence of processes themselves are very informative, *e.g.*, if a ground state bleach does not fully recover, it suggests the original molecule is not reforming on the timescale of the experiment. Quantitatively TAS are typically analysed under two models, (*i*) *simultaneous dynamics* or (*ii*) *sequential dynamics*[39].

(*i*) Most dynamical processes occurring during the relaxation of a molecule can be adequately described through first-order kinetics. This means a single exponential decay with some characteristic *lifetime* describes one process. Experimentally things are a bit more complicated because of nonlinear processes occurring around pump-probe overlap (time-zero), *e.g.* multiphoton effects in the sample cell, referred to as the instrument response function. This is typically well modelled by a Gaussian function with a full-width at half maximum in the region of $\sim$100 fs which ultimately limits the time resolution of the experiment. Together,

this means a general TAS under simultaneous dynamics can be modelled as the sum of n exponential decay functions with lifetimes τ_n, convoluted with a Gaussian instrument response function $\mathrm{G}(\lambda, \Delta t)$:

$$\mathrm{TAS}_{model}(\lambda, \Delta t) = \sum_{i}^{n} \mathrm{G}(\Delta t) \otimes \mathrm{A}_i(\lambda) e^{\frac{-(\Delta t - t_0)}{\tau_i}}, \tag{2}$$

where $\mathrm{A}_i(\lambda)$ is called the decay associated spectrum (DAS) for the corresponding exponential decay function with lifetime τ_i, and t_0 denotes time-zero. Nonlinear regression can minimise the residuals between the experimental TAS and TAS_{model}, for a particular wavelength. This analysis can be extended to include all wavelengths of the TAS simultaneously, so-called *global fitting*, the result of which is the 'average' dynamics across the entire TAS. One potential issue with this analysis is that the model intrinsically assumes the *all* dynamics start at the same time. If the processes within a relaxation mechanism are far removed from one another, *i.e.* occur on different timescales this assumption is adequate. However, for dynamical processes very close in magnitude this assumption breaks down and sequential dynamics become important.

(*ii*) Sequential dynamics use a kinetic model for the TAS where each process leads onto the next. This solves the problem of two or more dynamical processes being close in magnitude but requires the formation of a suitable model, where complexity rapidly increases when one process may 'branch' into multiple processes, something that has to be known before fitting of the TAS can be achieved. Often these models are formed on chemical intuition or following *ab initio* electronic structure calculations to inform on the likely model.

Either of these fitting methods can model a TAS and thus extract the lifetimes of the processes occurring following photoexcitation of the molecule of interest. Choosing a method of fitting will depend on the situation; whilst simultaneous dynamics can reveal very useful information, if sequential dynamic fitting is possible, it is ultimately always more representative of the actual relaxation mechanism. This experiment and subsequent analysis can reveal processes with lifetimes as small as ∼100 fs. The issue remains in assigning lifetimes to physical processes *e.g.* IC, ISC, photoproduct formation *etc.* With sensible assignment, the relaxation mechanism of a molecule and the timescale it occurs on may be deduced. In the next section we focus on two specific examples of sunscreen molecules where this experiment and analysis has been performed; oxybenzone a commonly used commercial sunscreen and sinapoyl malate a biological sunscreen deposited in plant leaves, where transient absorption spectroscopy has helped deduce the relaxation mechanism for each molecule.

3 Application to sunscreens

3.1 Oxybenzone

As briefly discussed in the Section 1.2, a prominent example of an organic filter used in commercial sunscreens is oxybenzone. It has been included in many sunscreen products since the 1980s and its job is predominately a UV-B absorber, but it does exhibit photoprotective properties into the UV-A region as well, making it a broadband UV absorber [23]. In commercial sunscreen products, the concentration of oxybenzone is regulated throughout Europe, the United States, Australia and Japan where each regulatory body sets a maximum allowed concentration, currently between 5–10% depending on the region [40–42]. This regulation comes amidst controversy over whether oxybenzone might cause adverse dermatological effects or alter the body's physiology. For example, some studies suggest that oxybenzone may cause contact dermatitis or disrupt the endocrine system [23]. There is however little literature in which discusses *how* oxybenzone provides its photoprotection. If this is understood, it may help in understanding how to reduce adverse effects of oxybenzone, or increase its efficacy as a sunscreen, a recent example of this utilises zeolite encapsulation and is shown to reduce adverse dermatological effects [11;43].

First and foremost, oxybenzone (OB) is a broadband UV absorber in the region 240–340 nm, as clearly shown from its UV-visible absorption spectrum, see Figure 7. It exists preferentially in a *enol*-isomer configuration but the transfer of a hydrogen atom to a neighbouring oxygen atom can form a less energetically stable, *keto*-isomer, see Figure 7. Recent *ab initio* electronic structure calculations suggest that ultrafast dynamics may be at the heart of OB's ability to provide efficient photoprotection [27]. Specifically, calculations have pointed towards an excited state hydrogen transfer, causing an isomerisation from the initial *enol*-isomer into the *keto*-isomer and subsequent IC from excited electronic states to the ground state to be a plausible relaxation mechanism. Given the processes suggested, the timescales involved

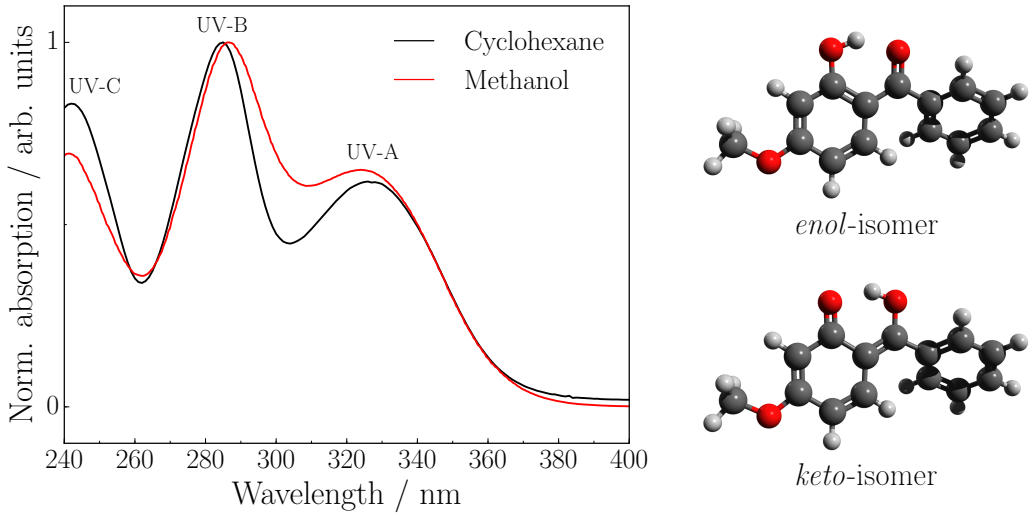

Figure 7: (*left*) UV-visible absorption spectrum of OB in the nonpolar solvent cyclohexane (black line) and the polar solvent methanol (red line) [44]. There are three clear absorption maxima in the UV-A, UV-B and UV-C regions. (*right*) OB exists preferentially in the more stable *enol*-isomer than the *keto*-isomer.

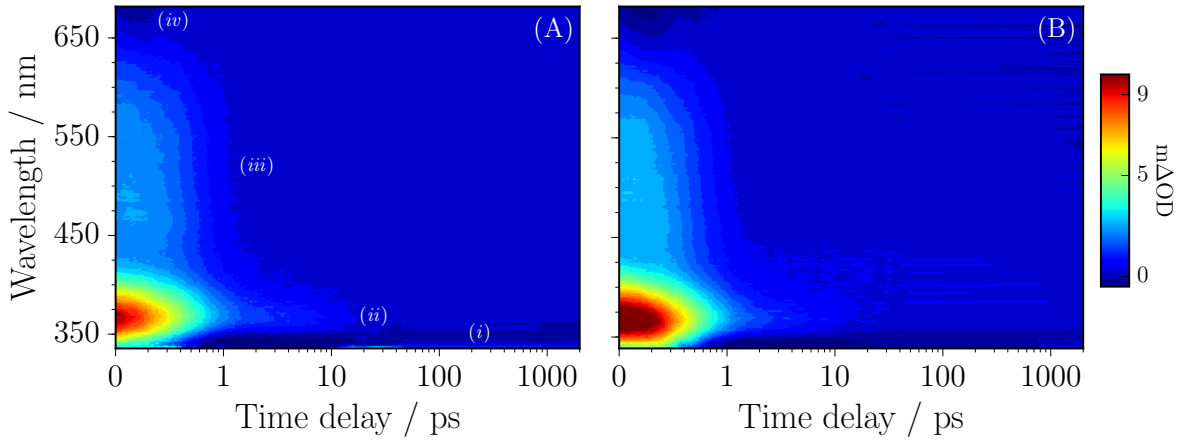

Figure 8: (A) TEA spectrum of OB in cyclohexane following an initial photoexcitation at ∼325 nm, in the form of a colourmap indicating the change in optical density. There are four main features observed in the TEA spectrum which have been labelled. (*i*) A negative feature below ∼350 nm which remains out to the maximum available pump-probe delay time of $\Delta t = 2$ ns. (*ii*) A localised, intense absorption feature centred on ∼366 nm which decays away by Δt ∼20 ps. (*iii*) A flat broad absorption feature which spans the probe window from ∼425–650 nm which decays away by $\Delta t = 2$ ps. (*iv*) A small negative feature beyond ∼650 nm. Each of these features are described in the main text. (B) Similar features are observed for OB in methanol.

would be ultrafast *cf.* Table 1.

Experimentally, ultrafast transient electronic absorption spectroscopy (TEAS) and transient vibrational absorption spectroscopy (TVAS), as described in Section 2 have been shown to unravel the dynamics involved in OB's relaxation mechanism[24]. In this study 10 mM samples of OB in cyclohexane and OB in methanol (referred to as OB-cyclohexane and OB-methanol respectively), were photoexcited at the UV-A absorption maximum *ca.* 325 nm.

3.1.1 Transient electronic absorption

Considering the TEAS measurements first; recording ΔOD for probe wavelengths between ∼335–675 nm over a range of pump-probe time delays up to $\Delta t = 2$ ns, transient electronic absorption (TEA) spectra were obtained, see Figure 8. There are four clear features observed in both the OB-cyclohexane (Figure 8(A)) and OB-methanol (Figure 8(B)) TEA spectrum. A note on terminology here, TEA spectrum and the vibrational analogue transient vibrational absorption (TVA) spectrum are both examples of the more general TAS introduced in Section 2. A distinction however is made here for the subsequent discussion where both TEA and TVA spectra are discussed and need to be distinguished.

(*i*) A negative feature is observed below probe wavelengths of ∼350 nm. From the UV-visible absorption spectrum of OB (Figure 7), OB displays a large absorption cross section below ∼350 nm which means that upon photoexcitation, there will be less molecules to absorb in this spectral region leading to a negative ΔOD, thus this feature is assigned to a ground state bleach (GSB, *cf.* Figure 6). This feature persists out to the maximum available pump-probe time delay, $\Delta t = 2$ ns, which suggests that within the parameters of this experiment, OB does not completely reform in its *enol*-isomer ground state (discussed later).

Table 2: The extracted lifetimes, τ_1 and τ_2 for OB-cyclohexane and OB-methanol using global regression analysis. The third lifetime, τ_{pl}, is inferred from a signal plateau as described in the main text.

Lifetime	OB-cyclohexane	OB-methanol
τ_1 / fs	375 ± 13	368 ± 13
τ_2 / ps	7.8 ± 2.8	4.9 ± 1.9
τ_{pl} / fs	∼100	∼100

(*ii*) A localised, intense absorption peak is observed centred on ∼366 nm which persists out to Δt ∼20 ps. Recent *ab initio* electronic structure calculations guide the interpretation of this signal[27], where it is suggested that an initial photoexcitation leads to the population of the higher lying electronic state, S_2, from which this absorption feature likely originates from. Therefore this feature is attributed to an excited state absorption (ESA, *cf.* Figure 6).

(*iii*) A flat, broad absorption across the probe spectral region ∼425–650 nm is observed which decays away to the baseline by $\Delta t = 2$ ps. With a similar interpretation of *ab initio* calculations[27] this feature too is attributed to an ESA.

(*iv*) A negative feature is observed beyond the probe spectral region of ∼650 nm for early time delays (< 1 ps) which might originate from stimulated emission of an excited electronic state, predominately the S_1. This is suggested given that this feature does not persist past ∼1 ps, by which time IC to the S_1 would have taken place, and this feature would decay away (discussed later).

Qualitatively, the observation of features in the TEA spectra are quite informative, particularly if GSB or stimulated emission signals are observed which can often give insight into the excited state potential energy surface or long-time fate of a molecule. In the case of OB, a conclusion can already be drawn from the incomplete recovery of the GSB, signalling the formation of a photoproduct. Quantitatively, the dynamical processes which occur in the TEA spectra may be modelled in order to extract the lifetime, that is, the timescales of each process. In the case of OB, a global nonlinear regression analysis[45] is used to extract the lifetimes of the dynamical processes involved in the relaxation mechanism, *cf.* Section 2.2 and Eq. 2. Two exponential decay functions were required (*i.e.* $n = 2$) to fully described the TEA spectra. The probe spectral region between 355–415 nm is only considered, *i.e.* focussing only on the localised absorption peak (*ii*). Furthermore, no convolution with a Gaussian instrument response function was required since the fitting was only considered for $\Delta t >$ 120 fs (OB-cyclohexane) and $\Delta t >$ 130 fs (OB-methanol). The result of this fitting is two dynamical lifetimes which are summarised in Table 2. A third dynamical lifetime is *inferred* from a signal plateau at very short time delays (< 100 fs) which would be heavily convoluted with any instrument response in this experiment[25]. Figure 9 shows a representative example of the resulting fitting procedure for the ∼366 nm transient of the TEA spectra (Figure 8), the two decay components, τ_1 and τ_2 as well as their sum are shown. The signal plateau from which a third dynamical lifetime (τ_{pl}) is inferred, is most clearly seen for OB-methanol (Figure 9(B)).

Now that the dynamical processes have been observed and quantified, the final step is to assign these processes to photophysical events involving the excited states of OB molecules.

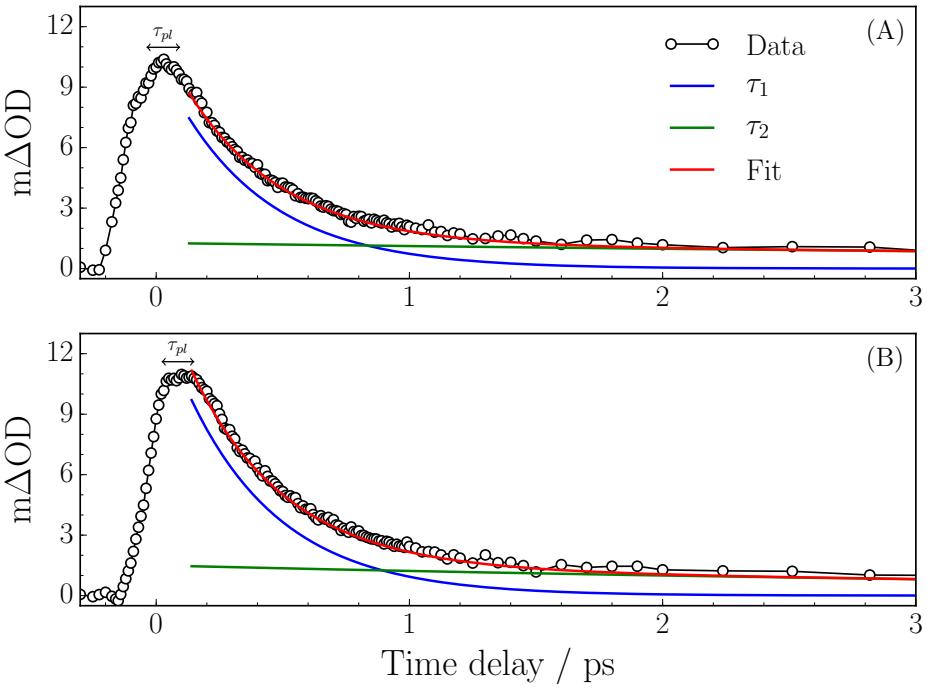

Figure 9: A representative example of the global fitting results. (A) For OB-cyclohexane, the ∼366 nm probe absorption transient is shown up to $\Delta t = 3$ ps. Two exponential decays functions with lifetimes, τ_1 (blue line) and τ_2 (green line) summed together (red line) describe the experimental data (black circles). (B) Similarly for the ∼366 nm transient of OB-methanol. As described in the main text, a plateau in the absorption feature can be seen, τ_{pl}, with duration closely matching the instrument response function, most clearly seen for OB-methanol.

Here recent *ab initio* calculations are invaluable in assigning these processes[27]. The pump photoexcitation excites OB molecules to a $S_2(1^1\pi\pi^*)$ state. Calculations suggest there is a barrierless pathway to a $S_1(1^1n\pi^*)$ state *via* a conical intersection (CI; a nonadiabatic crossing between multiple potential energy surfaces[46]) meaning OB may undergo IC from S_2 to S_1. Following this, hydrogen transfer from the hydroxyl group to the neighbouring oxygen, referred to as excited state hydrogen transfer, is suggested to occur forming the *keto*-isomer. These processes are attributed to the shortest lifetime, the signal plateau τ_{pl} of ∼100 fs (Figure 9).

Now in the S_1 state, the *keto*-isomer of OB is suggested to undergo a geometry change where the phenoxyl rings rotate around the central aliphatic C−C bond, resulting in a twisted geometry[24]. This allows OB to couple to the ground electronic state, S_0 through another CI. This is attributed to the lifetime τ_1 and sensibly compares to similar systems where *enol*–*keto* isomerisation is observed[47;48]. Of course, given the nature of simultaneous dynamics where all processes are assumed to onset from the start (*cf.* Section 2.2), and the timescales involved, it is not definitive that τ_1 and τ_{pl} are distinguishable in the way described thus far. A possibility remains that τ_{pl} might capture the IC from S_2 to S_1 only. In this case τ_1 would capture the excited state hydrogen transfer and the geometry change.

After IC to the S_0 state, OB undergoes a reverse isomerisation *i.e. keto* → *enol*, referred to as a ground state hydrogen transfer. This leaves the *enol*-OB isomer in an energetic vibra-

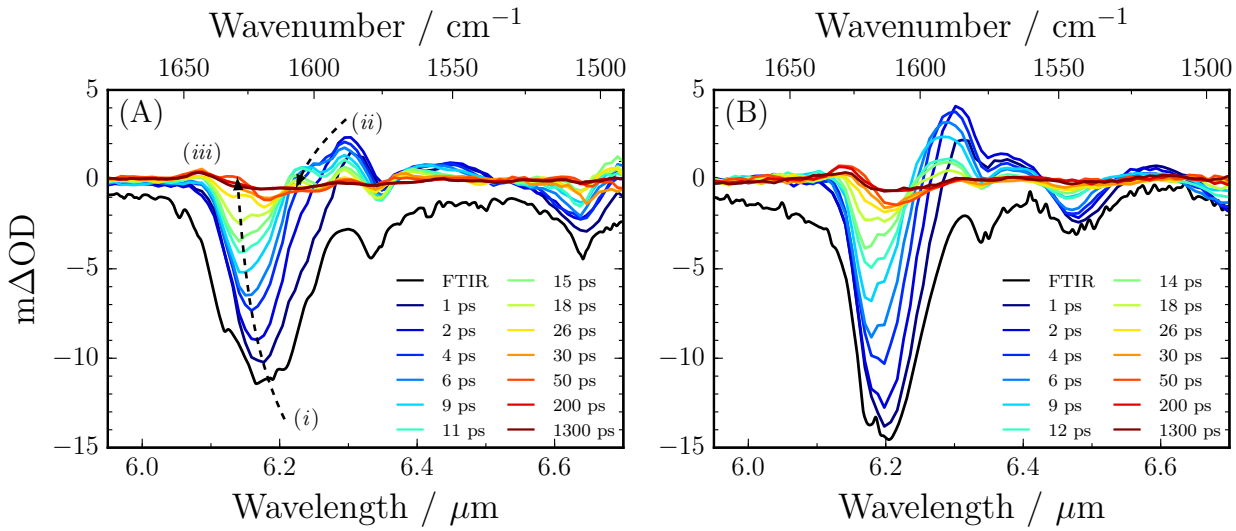

Figure 10: TVA spectra for a range of pump-probe time up to Δt = 1.3 ns. (A) For OB-cyclohexane, the TVA spectrum is dominated by three features. (*i*) An intense GSB feature centred around ∼6.2 μm, which decays and shifts to shorter wavelengths with increasing Δt, but does not fully recover by Δt = 1.3 ns. (*ii*) A positive absorption centred around ∼6.3 μm. (*iii*) Another positive absorption feature is observed centred around ∼6.1 μm. (B) Similar features are observed in the TVA spectrum of OB-methanol.

tional state which subsequently distributes this energy to the surrounding solvent molecules (cyclohexane or methanol), recovering the ground state *enol*-isomer, and completing the relaxation mechanism. This final processes is attributed the lifetime τ_2. Contrary to τ_1 where the lifetime is the same for cyclohexane and methanol measurements, τ_2 is solvent dependent. Importantly, OB exhibits a faster rate of vibrational energy transfer (VET) in the more polar solvent methanol than in the nonpolar cyclohexane *cf.* 4.9 ps to 7.8 ps respectively, consistent with a greater degree of hydrogen bonding[49].

3.1.2 Transient vibrational absorption

In support of the TEAS measurements and the assignment of photophysical processes, TVAS measurements are also taken. The subtle but important difference is that the probe pulses are in the infrared region, ∼5.9–6.7 μm (1 μm = 1000 nm) *cf.* ∼335–675 nm in TEAS measurements, which excite vibrational modes within OB. The advantage of this technique over TEAS is that the formation or destruction of bonds can be tracked, whereas in TEAS only the changes in electronic states are observed. The result of these measurements are TVA spectra for OB-cyclohexane and OB-methanol given in Figure 10(A) and 10(B) respectively.

Considering OB-cyclohexane first (Figure 10(A)), the spectrum is dominated by several GSB features from the earliest pump-probe time delays (1 ps), and matches the static Fourier transform infrared (FTIR; black line) spectrum (the UV-visible spectrum equivalent in TEAS measurements). The most intense GSB contribution is observed at ∼6.2 μm labelled (*i*). This feature shifts to shorter wavelengths for increased time delay (Figure 10(A), dashed line). A positive absorption feature is also seen to the longer wavelength side of this GSB feature, labelled (*ii*), centred at ∼6.3 μm. Similarly this feature can be seen to shift towards shorter wavelengths for an increased time delay up to Δt = 10 ps. Qualitatively, the temporal

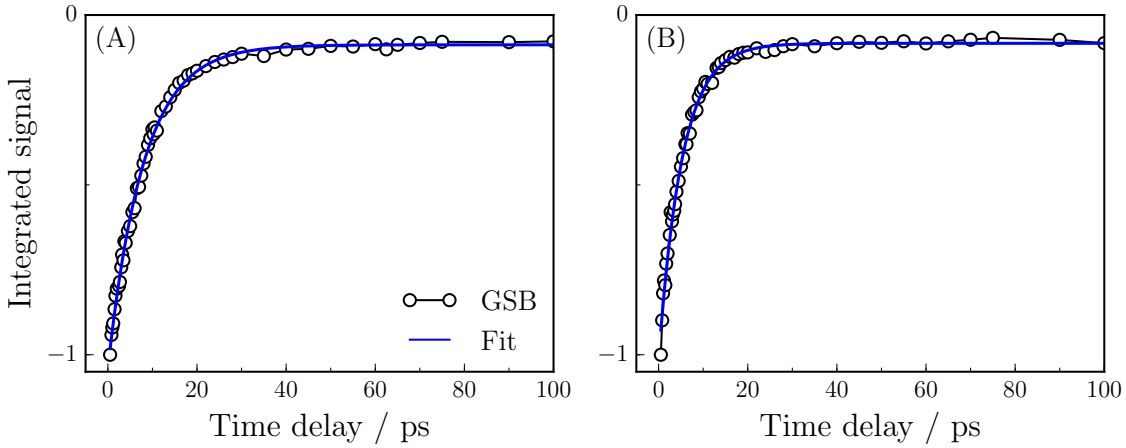

Figure 11: The kinetic trace of the integrated peak centred at ∼6.2 μm for increasing pump-probe time delay (black circles) of (A), OB-cyclohexane and (B) OB-methanol. The kinetic traces are well described by a single exponential decay (blue line) with lifetime $\tau = 8.0 \pm 0.2$ ps and $\tau = 5.2 \pm 0.2$ ps for OB-cyclohexane and OB-methanol respectively.

behaviour of this feature is characteristic of a vibrationally energetic molecule transferring excess energy to a surrounding solvent, consistent with the last step observed in TEAS measurements (*cf.* τ_2)[38]. Similar features are observed for OB-methanol (Figure 10(B)).

Quantitatively, feature (*i*) can be analysed by numerical integration of the peak at each time delay[38]. The resultant fitting of this is a kinetic trace, given in Figure 11. The kinetic trace for both OB-cyclohexane and OB-methanol are well described by a single exponential decay function, with lifetime, $\tau = 8.0 \pm 0.2$ ps and $\tau = 5.2 \pm 0.2$ ps respectively suggesting the time taken for overall relaxation process is in very good agreement with the τ_2 lifetime determined by the TEAS measurements.

Finally, the GSB feature (*i*) does not fully recover at the maximum available time delay, $\Delta t = 1.3$ ns, suggesting a quantum yield for a photoproduct of ϕ ∼10%. This is investigated through *ab initio* calculations of the harmonic frequencies of likely candidates for the photoproduct which are compared to the experimental TVA spectra, labelled (*iii*)[24], centred around ∼6.1 μm. The conclusion of these calculations and subsequent analysis points to the likely photoproduct being a long-lived *keto*-isomer which has undergone significant excess rotation about the aliphatic C−C bond, referred to as a trans *keto*-isomer, *vide infra*. Similar studies have also observed the generation of a photoproduct and have attributed it to the formation of a phenoxyl radical after O−H bond fission[26].

Thus TVAS measurements have not only complemented TEAS measurements, where the timescales of identified processes are in very good agreement, each has provided something unique. TEAS measurements have identified two sub picosecond dynamical components in addition to the longer picosecond component both TEAS and TVAS identified. TVAS on the other hand has provided a likely candidate of the photoproduct, which TEAS is unable to do. These two techniques have provided a complete, plausible relaxation mechanism of OB after UV-A excitation. Studies have gone on to confirm that OB behaves similarly for photoexcitation at the UV-B and UV-C regions[25], with the suggested relaxation mechanism summarised in Figure 12. Taken all together, these investigations conclude that OB displays a broadband, ultrafast photoprotective properties, which photophysically justifies its inclusion

in commercial sunscreen products.

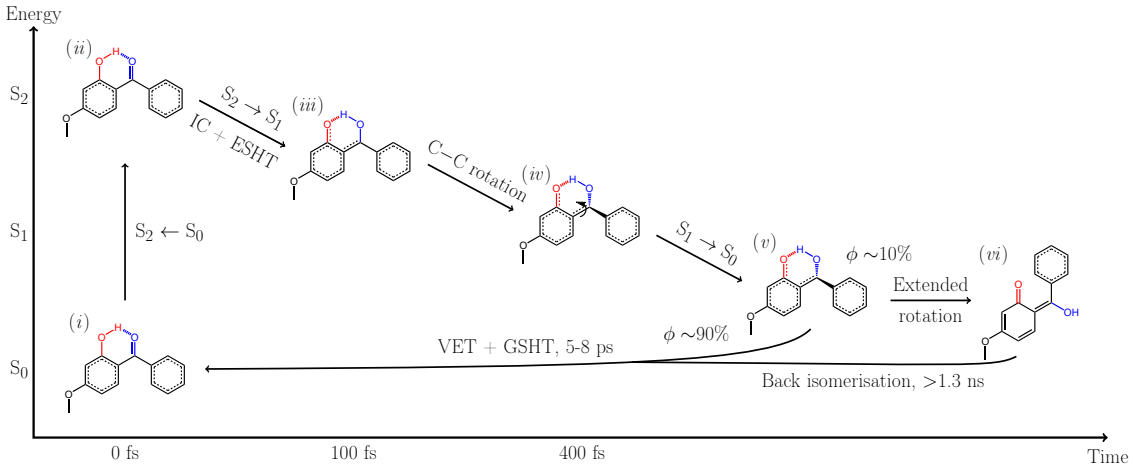

Figure 12: Summary of the proposed relaxation mechanism OB displays after UV-A (also UV-B and UV-C)[25] photoexcitation, as determined by TEAS and TVAS[24]. (*i*) OB exists preferentially in the more stable *enol*-isomer. (*ii*) UV-A radiation photoexcites OB to $S_2(1^1\pi\pi^*)$ state. (*iii*) After ∼100 fs, OB undergoes internal conversion (IC) and excited state hydrogen transfer (ESHT) forming the *keto*-isomer in the $S_1(1^1n\pi^*)$ state. (*iv*) Over the next ∼400 fs, OB undergoes a rotation about its central aliphatic C−C bond. (*v*) This geometry allows the S_1 state to couple to the S_0 state, where OB undergoes vibrational energy transfer (VET) to the surrounding solvent and ground state hydrogen transfer (GSHT) to reform the original ground state *enol*-isomer with a quantum yield of ϕ ∼90%. (*vi*) The remaining ∼10% of OB molecules may undergo further C−C bond rotation locking the molecules in a long-lived trans *keto*-isomer. This photoproduct lives for the duration of the experiment, thus remains stable for at least 1.3 ns (from TVAS measurements).

3.2 Sinapoyl malate

Aside from commercial sunscreens, TEAS has been utilised to investigate how biological sunscreens provide the photoprotection nature has selected them for[50]. An example of this is sinapoyl malate, a molecule highly suspected to fulfil the role of a sunscreen[16;51;52] which is deposited in the upper epidermis of the leaves of many plants. As described in Section 1.1.2, the phenylpropanoid pathway is responsible for regulating the concentration of important metabolites, such as sinapate esters, from which sinapoyl malate is a derivative of. A similar methodology is employed to understand the relaxation mechanism of sinapoyl malate after UV irradiation as was discussed for oxybenzone.

Sinapoyl malate (SM) absorbs UV radiation strongly across the UV-A and UV-B regions, see Figure 13. It may exist as either a *trans* or *cis* isomer with the former being energetically more preferable. Understanding how SM relaxes after UV absorption will not only help to understand biological photoprotection in many plants, but might lend lessons in developing commercial sunscreens with improved dermatological properties or energy dissipation efficacy. Experimentally, 1 mM SM in the nonpolar aprotic solvent dioxane, the polar aprotic solvent acetonitrile (ACN) or the polar protic solvent methanol is photoexcited at ∼330 nm, *cf.* absorption maxima of Figure 13.

Considering the TEAS measurements of SM-dioxane first; recording ΔOD for probe wavelengths between ∼335–675 nm over a range of pump-probe time delays up to $\Delta t = 2$ ns a TEA spectrum is obtained, see Figure 14(A). The TEA spectrum displays three main absorption features.

(*i*) The first is a negative feature observed below probe wavelengths of ∼360 nm which persists out to the maximum pump-probe time delay of $\Delta t = 2$ ns. Comparing to the static UV-visible spectrum of SM (Figure 13), this feature is assigned to a GSB. Qualitatively, this points to a incomplete recovery of ground state *trans*-isomer SM molecules suggesting the

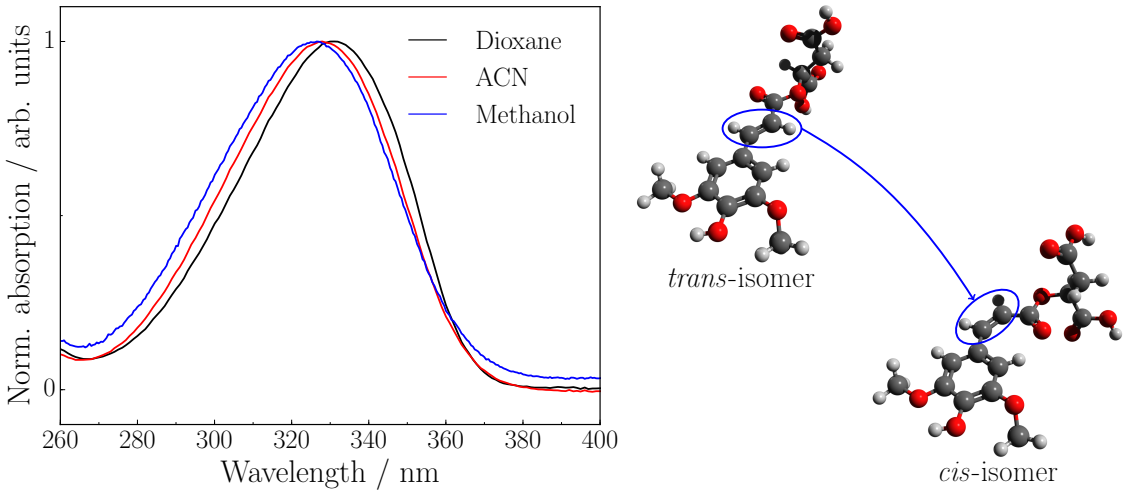

Figure 13: (*left*) UV-visible absorption spectrum of SM in the nonpolar aprotic solvent dioxane (black line), the polar aprotic solvent ACN (red line) and the polar protic solvent methanol (blue line). The UV absorption maxima lie to the short wavelength side of the UV-A region, *ca.* 329, 328 and 326 nm for dioxane, ACN and methanol respectively. (*right*) SM exists preferentially in the more energetically stable *trans*-isomer. The less stable *cis*-isomer is shown for completeness.

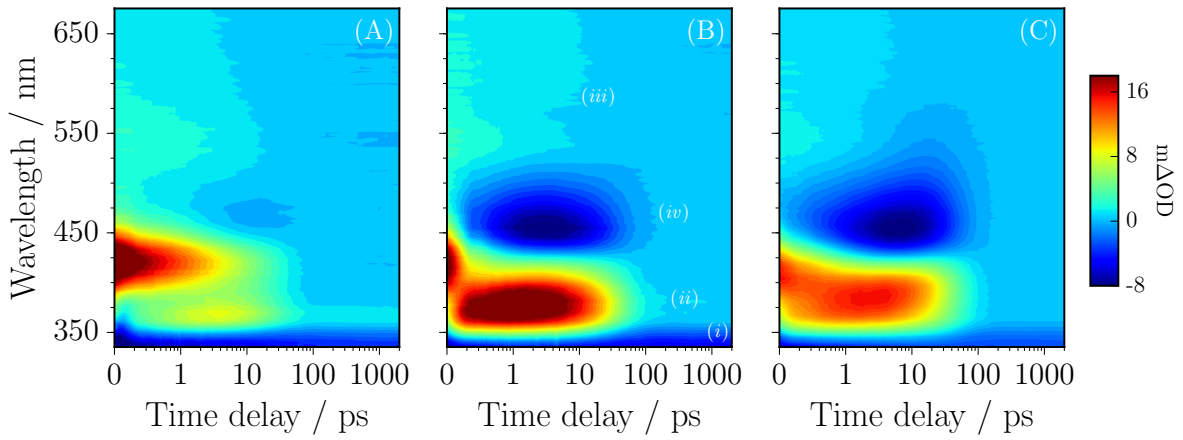

Figure 14: (A) TEA spectrum of SM in dioxane following an initial photoexcitation at 329 nm, in the form of a colourmap indicating ΔOD. There are three main features observed in the TEA spectrum which have been labelled in (B). (*i*) A negative feature below ∼360 nm which remains out to the maximum available pump-probe time delay of Δt = 2 ns. (*ii*) A localised, intense absorption feature centred on ∼420 nm which decays away by Δt ∼100 ps. (*iii*) A flat broad absorption feature which spans the probe window from ∼420–650 nm which decays away by Δt = 10 ps. (B-C) Similar features are observed for SM in ACN and methanol respectively with these two addenda. A strong negative feature (*iv*) appears centred at ∼460 nm which decays away by ∼100 ps. The localised absorption seen in dioxane centred at ∼420 nm now appears blue-shifted at ∼370 nm.

formation of a photoproduct.

(*ii*) A localised, intense absorption peak is centred on ∼420 nm which decays away by Δt = 50 ps. Since photoexcitation around ∼320 nm promotes a $1^1\pi\pi^*$ transition, this feature is assigned to ESA of the excited $1^1\pi\pi^*$ state based on *ab initio* calculations for similar molecular systems[27].

(*iii*) Finally, a broad absorption feature is observed beyond ∼420 nm and spanning the probe spectral region. With a similar rationale for the (*ii*) absorption feature, this feature is also attributed to ESA of the excited $1^1\pi\pi^*$ state.

Similar observations are made for TEAS measurements of SM-ACN and SM-methanol with the following addenda: the intense localised absorption feature (*ii*) is blue-shifted and centred instead on ∼370 nm. A fourth absorption feature is also observed which is not present in SM-dioxane measurements:

(*iv*) A strong negative absorption feature is observed centred at ∼460 nm. It persists out to Δt ∼100 ps and is attributed to stimulated emission from a $2^1\pi\pi^*$ state, given the likely excited states involved based on similar molecular systems[27;53].

Quantitatively, the dynamical processes which occur with the TEA spectra are modelled using global nonlinear regression analysis[45]. With reference to Section 2.2 and Eq. 2, three exponential decay functions were required (*i.e.* $n = 3$) to fully described the TEA spectra. The entire probe spectral region, ∼335–675 nm is considered as well as convolution with a Gaussian instrument response function, with full-width at half maximum, G(Δt) ∼100 fs. The result of this fitting is three dynamical lifetimes which are summarised in Table 3.

The incomplete recovery of the GSB is investigated through the using UV-visible spectroscopy. A UV-visible spectrum is first taken of SM in each solvent (SM-solvent) referred

Table 3: The extracted lifetimes, τ_1, τ_2, τ_3 for SM-dioxane, SM-ACN and SM-methanol using global regression analysis.

Lifetime	SM-dioxane	SM-ACN	SM-methanol
τ_1 / fs	119 ± 28	51 ± 4	619 ± 101
τ_2 / ps	1.62 ± 0.15	0.63 ± 0.04	4.81 ± 0.77
τ_3 / ps	22.4 ± 1.9	27.3 ± 0.77	33.5 ± 1.7

to as the '*before spectrum*'. SM-solvent is then irradiated for 10 minutes using a lamp which emits UVR centred on the photoexcitation wavelengths used in TEAS measurements (*i.e.* 329, 328 or 326 nm), after which another UV-visible spectrum is taken, referred to as the '*after spectrum*'. The before spectrum is subtracted from the after spectrum to give a '*difference spectrum*', which highlights features that have formed or disappeared after UV irradiation. The result of this is given in Figure 15 (black lines). A clear absorption peak appears for all SM-solvent measurements centred at ∼370 nm which resembles the peak seen in the corresponding Δt = 2 ns TEAS measurements (red lines). This indicates the photoproduct is long-lived, at least on the timescale of minutes. From measurements of similar molecules[54;55], this feature may be assigned to the formation of a stable *cis*-isomer. Discrepancies between the difference spectrum and Δt = 2 ns transient is observed for SM-ACN and SM-methanol, see Figure 15(B) and 15(C). (*i*) The *cis*-isomer peak at ∼370 nm becomes broader on the red-wavelength side. (*ii*) At wavelengths above ∼400 nm, a clear absorption across the probe window is seen. (*i*) Is attributed to the formation of a radical through two-photon ionisation based on previous studies[56;57] whereas (*ii*) is attributed to possible triplet state formation[58] which in both cases is amplified in the more polar protic solvent methanol.

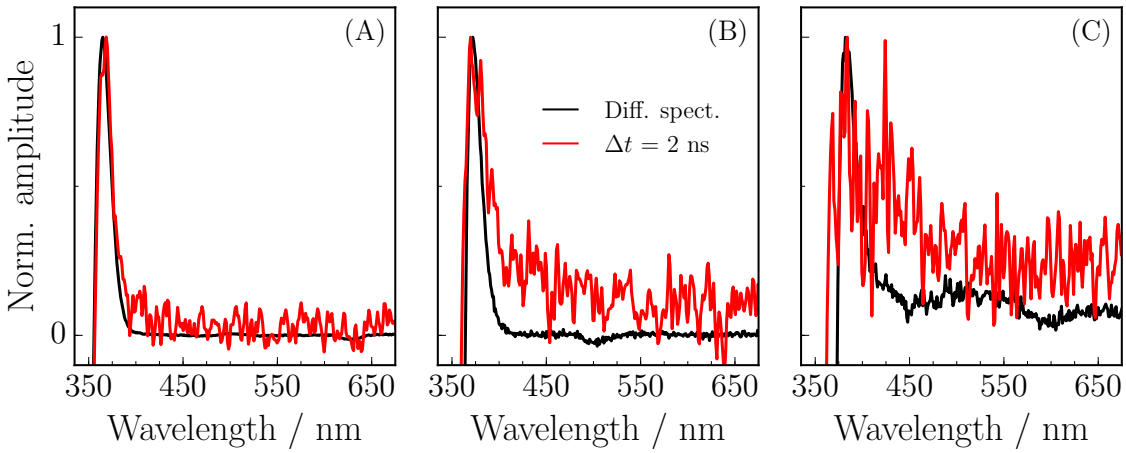

Figure 15: (A) Difference spectrum of SM-dioxane after 10 minutes UV irradiation (black line) as described in the main text, compared to the Δt = 2 ns transient from TEAS measurements (red line). A clear absorption peak emerges after UV irradiation and is present in the Δt = 2 ns transient. (B-C) Similar observations are made for SM-ACN and SM-methanol respectively. However in these measurements there is a clear absorption spanning the probe window in the Δt = 2 ns transients compared to their respective difference spectra which suggests the formation of another photoproduct.

Assigning these dynamical lifetimes to specific photophysical processes is the final task. The initial photoexcitation event promotes SM molecules to their $1^1\pi\pi^*$ state[27]. From here, it is suggested τ_1 and τ_2 describe multiple processes which are convoluted together. This has the effect of 'blurring' one process with another making the absolute assignment of any one process with any one lifetime difficult. Overall however, τ_1 is suggested to describe an early time Δt <100 fs coherent artefact from the instrument response function, as well as any evolution out of the Franck-Condon window. Following this, propagation to a $2^1\pi\pi^*$ state is suggested to occur, thus IC *via* a $1^1\pi\pi^*/2^1\pi\pi^*$ CI, along with any solvent rearrangement, is described by τ_2 which sensibly compares to related molecular systems[53;56;59]. Of course it should be noted that these lifetimes in particular will be most effected by the formation of the radical species and triplet state absorption. Propagation along the $2^1\pi\pi^*$ potential energy surface to a $2^1\pi\pi^*/S_0$ CI enables the excited state SM molecules to couple back to the ground state, and relax *via* vibrational energy transfer to the surrounding solvent. These final steps are captured by the lifetime τ_3. As shown, some of the molecules can relax into a stable *cis*-isomer configuration instead of flowing through the $2^1\pi\pi^*/S_0$ CI. A summary of this suggested mechanism is given in Figure 16.

Thus ultrafast dynamics are observed and quantified which directly explains why SM behaves as an efficient sunscreen. A *cis*-isomer photoproduct is observed and minimal radical and triplet state formation are observed. In the case of radical formation through a two-photon ionisation process, it would be unlikely to occur in nature given the intensity of light from the sun incident on plant leaves. Photophysically SM is justified as an efficient biological sunscreen.

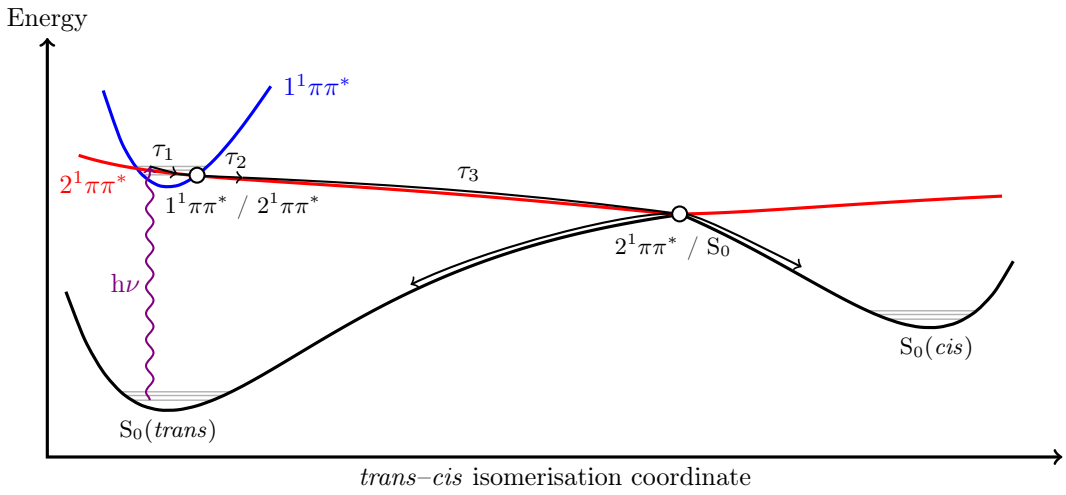

Figure 16: The overall proposed mechanism SM displays after UV-A photoexcitation. An initial photoexcitation populates the $1^1\pi\pi^*$ state. From here SM undergoes geometry relaxation out of the Franck-Condon window, captured by τ_1. Propagation onto a $2^1\pi\pi^*$ state *via* a CI is described by τ_2. A $2^1\pi\pi^*/S_0$ CI allows SM to couple back to the ground state where vibrational energy transfer to the surrounding solvent recovers the ground state, captured by τ_3. A small proportion of the excited state population can become trapped in a long-lived stable *cis*-isomer. Triplet state absorption has been omitted for simplicity.

4 Outlook

This review began with a overview of the common photophysical processes which follow photoexcitation, the typical timescales of which require ultrafast experimental resolution. Sunscreens are a class of molecules which typically exhibit these processes in order to absorb harmful ultraviolet light from the sun, before it has chance to damage sensitive tissue in the skin. Transient absorption spectroscopy (transient electronic absorption spectroscopy and the complementary vibrational analogue) is discussed as a suitable technique to use, where solution phase measurements provide a first step in building the complexity of a typical commercial sunscreen. Two case studies are presented, oxybenzone, a common ingredient in commercial sunscreens, and sinapoyl malate, a biological sunscreen found in many plant leaves. Transient absorption spectroscopy is shown to provide valuable qualitative information about the electronic transitions involved, as well as indicating the presence of long-lived photoproducts. Quantitatively, global nonlinear regression analysis is one of a number of techniques which can provide detailed quantitation of the lifetimes of the likely photophysical processes occurring in the molecules. Numerous ultrafast processes are shown to be at play in both oxybenzone and sinapoyl malate, explaining how both these molecules fulfil their roles as efficient sunscreening molecules. Coupled with other techniques, like UV-visible spectroscopy, vibrational spectroscopy and *ab initio* electronic structure calculations provide an extension to the analysis of possible photoproducts identified in transient absorption spectroscopy, typically by the incomplete recovery of a ground state bleach.

Of course, there is much more to these molecules than the techniques presented here are capable of resolving. For example, how do these molecules behave when in solution or the condensed phase with other sunscreen molecules? - as they are typically found in commercial sunscreens. What happens at very early delay times *i.e.* < 100 fs within the instrument response function of these experiments? - detailed quantum mechanical and molecular mechanics simulations can begin to answer these questions[60]. Further afield many questions about the suitability of these molecules on human skin and the human physiology are still unanswered *i.e.* the so-called sunscreen controversy - these questions will require interdisciplinary collaboration *e.g.* clinical studies to be understood.

Transient absorption spectroscopy has been shown as an important tool in answering some of these questions, providing detailed quantitative information of key photophysical processes occurring in sunscreen molecules. This information might find use in designing new sunscreen formulations or even improving existing ones. In an age where malignant melanoma cases are on the rise, the availability of travel and tourism increasing and shifting attitudes towards sun exposure and skin care have been rapidly changing, confronting the sunscreen controversy on the molecular scale has become increasingly important.

5 Acknowledgements

L.A.B. thanks the Engineering and Physical Sciences Research Council (EPSRC) for providing a studentship under grant EP/F500378/1, through the *Molecular Organisation and Assembly in Cells Doctoral Training Centre*. V.G.S thanks the Royal Society for a University Research Fellowship.

References

[1] Sagan, C. *J. Theor. Biol.* **1973**, *39*, 195–200.

[2] Hessen, D. O. Solar radiation and the evolution of life. Solar radiation and human health. 2008; pp 123–136.

[3] Holick, M. F. *Am. J. Clin. Nutr.* **2004**, *80*, 1678S–1688S.

[4] Caldwell, M. M.; Bornman, J. F.; Ballaré, C. L.; Flint, S. D.; Kulandaivelu, G. *Photochem. Photobiol. Sci.* **2007**, *6*, 252–266.

[5] Lucas, R.; McMichael, T.; Smith, W.; Armstrong, B. *Solar Ultraviolet Radiation. Global burden of disease from solar ultraviolet radiation*; Environmental Burden of Disease Series, No. 13; World Health Organization: Geneva, 2006.

[6] Lucas, R. M.; Ponsonby, A.-L. *Med. J. Aust.* **2002**, *177*, 594–598.

[7] Organization, W. H. Health effects of UV radiation. accessed March 2016; http://www.who.int/uv/health/en/.

[8] Holick, M. F. *N. Engl. J. Med.* **2007**, *357*, 266–281.

[9] Mason, R. S.; Reichrath, J. *Anticancer Agents Med. Chem.* **2013**, *13*, 83–97.

[10] Cichorek, M.; Wachulska, M.; Stasiewicz, A.; Tymińska, A. *Postępy. Dermatol. Alergol.* **2013**, *30*, 30–41.

[11] Ortonne, J. P. *Br. J. Dermatol.* **2002**, *146*, 7–10.

[12] Eller, M. S.; Gilchrest, B. A. *Pigment Cell Res.* **2000**, *13*, 94–97.

[13] Levine, J. A.; Sorace, M.; Spencer, J.; Siegel, D. M. *J. Am. Acad. Dermatol.* **2005**, *53*, 1038–1044.

[14] Jenkins, G. I. *Annu. Rev. Plant Biol.* **2009**, *60*, 407–431.

[15] Frohnmeyer, H.; Staiger, D. *Plant Physiol.* **2003**, *133*, 1420–1428.

[16] Fraser, C. M.; Chapple, C. *Arabidopsis Book* **2011**, *9*, e0152.

[17] Kasparian, N. A.; McLoone, J. K.; Meiser, B. *J. Behav. Med.* **2009**, *32*, 406–428.

[18] Forestier, S. *J. Am. Acad. Dermatol.* **2008**, *58*, S133–S138.

[19] Dransfield, G. P. *Radiation Protection Dosimetry* **2000**, *91*, 271–273.

[20] Frisch, M. J. et al. Gaussian 03, Revision D.01. Gaussian, Inc., Wallingford, CT, 2004.

[21] Hanwell, M. D.; Curtis, D. E.; Lonie, D. C.; Vandermeersch, T.; Zurek, E.; Hutchison, G. R. *J. Cheminf.* **2012**, *4*, 1–17.

[22] Persistence of Vision (TM) Raytracer. 2004; http://www.povray.org/.

[23] Burnett, M. E.; Wang, S. Q. *Photodermatol. Photoimmunol. Photomed.* **2011**, *27*, 58–67.

[24] Baker, L. A.; Horbury, M. D.; Greenough, S. E.; Coulter, P. M.; Karsili, T. N. V.; Roberts, G. M.; Orr-Ewing, A. J.; Ashfold, M. N. R.; Stavros, V. G. *J. Phys. Chem. Lett.* **2015**, *6*, 1363–1368.

[25] Baker, L. A.; Horbury, M. D.; Greenough, S. E.; Ashfold, M. N. R.; Stavros, V. G. *Photochem. Photobiol. Sci.* **2015**, *14*, 1814–1820.

[26] Ignasiak, M. T.; Houée-Levin, C.; Kciuk, G.; Marciniak, B.; Pedzinski, T. *ChemPhysChem* **2015**, *16*, 628–633.

[27] Karsili, T. N. V.; Marchetti, B.; Ashfold, M. N. R.; Domcke, W. *J. Phys. Chem. A* **2014**, *118*, 11999–12010.

[28] Valeur, B. *Molecular Fluorescence: Principles and Applications*; Wiley-VCH, Weinheim, 2002.

[29] Scherer, N. F.; Knee, J. L.; Smith, D. D.; Zewail, A. H. *J. Phys. Chem.* **1985**, *89*, 5141–5143.

[30] Dantus, M.; Rosker, M. J.; Zewail, A. H. *J. Chem. Phys.* **1987**, *87*, 2395–2397.

[31] Zewail, A. H. *Pure Appl. Chem.* **2000**, *72*, 12.

[32] Young, J. D.; Staniforth, M.; Paterson, M. J.; Stavros, V. G. *Phys. Rev. Lett.* **2015**, *114*, 233001.

[33] Berera, R.; van Grondelle, R.; Kennis, J. T. M. *Photosynth. Res.* **2009**, *101*, 105–118.

[34] Quan, W.-D.; Pitto-Barry, A.; Baker, L. A.; Stulz, E.; Napier, R.; O'Reilly, R. K.; Stavros, V. G. *Chem. Commun.* **2016**, *52*, 1938–1941.

[35] Greenough, S. E.; Roberts, G. M.; Smith, N. A.; Horbury, M. D.; McKinlay, R. G.; Żurek, J. M.; Paterson, M. J.; Sadler, P. J.; Stavros, V. G. *Phys. Chem. Chem. Phys.* **2014**, *16*, 19141–19155.

[36] Keller, U. *Nature* **2003**, *424*, 831–838.

[37] Boyd, R. W. *Nonlinear Optics*, 3rd ed.; Academic Press: Burlington, 2008.

[38] Roberts, G. M.; Marroux, H. J. B.; Grubb, M. P.; Ashfold, M. N. R.; Orr-Ewing, A. J. *J. Phys. Chem. A* **2014**, *118*, 11211–11225.

[39] van Stokkum, I. H.; Larsen, D. S.; van Grondelle, R. *Biochim. Biophys. Acta* **2004**, *1657*, 82–104.

[40] Osterwalder, U.; Sohn, M.; Herzog, B. *Photodermatol. Photoimmunol. Photomed.* **2014**, *30*, 62–80.

[41] Lodén, M.; Beitner, H.; Gonzalez, H.; Edström, D.; Åkerström, U.; Austad, J.; Buraczewska-Norin, I.; Matsson, M.; Wulf, H. *Br. J. Dermatol.* **2011**, *165*, 255–262.

[42] Sambandan, D. R.; Ratner, D. *J. Am. Acad. Dermatol.* **2011**, *64*, 748–758.

[43] Chrétien, M. N.; Heafey, E.; Scaiano, J. C. *Photochem. Photobiol.* **2010**, *86*, 153–161.

[44] Hunter, J. D. *Comput. Sci. Eng.* **2007**, *9*, 90–95.

[45] Chatterley, A. S.; West, C. W.; Stavros, V. G.; Verlet, J. R. R. *Chem. Sci.* **2014**, *5*, 3963–3975.

[46] Yarkony, D. R. *Rev. Mod. Phys.* **1996**, *68*, 985–1013.

[47] Verma, P. K.; Steinbacher, A.; Koch, F.; Nuernberger, P.; Brixner, T. *Phys. Chem. Chem. Phys.* **2015**, *17*, 8459–8466.

[48] Barbatti, M.; Aquino, A. J. A.; Lischka, H.; Schriever, C.; Lochbrunner, S.; Riedle, E. *Phys. Chem. Chem. Phys.* **2009**, *11*, 1406–1415.

[49] Owrutsky, J. C.; Raftery, D.; Hochstrasser, R. M. *Annu. Rev. Phys. Chem.* **1994**, *45*, 519–555.

[50] Baker, L. A.; Horbury, M. D.; Greenough, S. E.; Allais, F.; Walsh, P. S.; Habershon, S.; Stavros, V. G. *J. Phys. Chem. Lett.* **2016**, *7*, 56–61.

[51] Chapple, C. C. S.; Vogt, T.; Ellisy, B. E.; Somerville, C. R. *Plant Cell* **1992**, *4*, 1413–1424.

[52] Ruegger, M.; Chapple, C. *Genetics* **2001**, *159*, 1741–1749.

[53] Mataga, N.; Chosrowjan, H.; Taniguchi, S.; Hamada, N.; Tokunaga, F.; Imamoto, Y.; Kataoka, M. *Phys. Chem. Chem. Phys.* **2003**, *5*, 2454–2460.

[54] Miyazaki, Y.; Inokuchi, Y.; Akai, N.; Ebata, T. *J. Phys. Chem. Lett.* **2015**, *6*, 1134–1139.

[55] Karpkird, T. M.; Wanichweacharungruang, S.; Albinsson, B. *Photochem. Photobiol. Sci.* **2009**, *8*, 1455–1460.

[56] Vengris, M.; van Stokkum, I. H. M.; He, X.; Bell, A. F.; Tonge, P. J.; van Grondelle, R.; Larsen, D. S. *J. Phys. Chem. A* **2004**, *108*, 4587–4598.

[57] Larsen, D. S.; van Stokkum, H. M.; Vengris, M.; van der Horst, M. A.; de Weerd, F. L.; Hellingwerf, K. J.; van Grondelle, R. *Biophys. J.* **2004**, *87*, 1858–1872.

[58] Horbury, M. D.; Baker, L. A.; Quan, W.-D.; Young, J. D.; Staniforth, M.; Greenough, S. E.; Stavros, V. G. *J. Phys. Chem. A* **2015**, *119*, 11989–11996.

[59] Vengris, M.; Larsen, D. S.; van der Horst, M. A.; Larsen, O. F. A.; Hellingwerf, K. J.; van Grondelle, R. *J. Phys. Chem. B* **2005**, *109*, 4197–4208.

[60] Marchetti, B.; Karsili, T. N. V. *Phys. Chem. Chem. Phys.* **2016**, *18*, 3644–3658.